A Review of an Old Dilemma: Demosaicking First, or Denoising First?

Qiyu Jin
School of mathematical science,
Inner Mongolia University
qyjin2015@aliyun.com

Gabriele Facciolo
Centre Borelli,
ENS Paris-Saclay, CNRS
facciolo@cmla.ens-cachan.fr

Jean-Michel Morel
Centre Borelli,
ENS Paris-Saclay, CNRS
moreljeanmichel@gmail.com

Abstract

Image denoising and demosaicking are the first two crucial steps in digital camera pipelines. In most of the literature, denoising and demosaicking are treated as two independent problems, without considering their interaction, or asking which should be applied first. Several recent works have started addressing them jointly in works that involve heavy weight neural networks, thus incompatible with low power portable imaging devices. Hence, the question of how to combine denoising and demosaicking to reconstruct full color images remains very relevant: Is denoising to be applied first, or should that be demosaicking first? In this paper, we review the main variants of these strategies and carry-out an extensive evaluation to find the best way to reconstruct full color images from a noisy mosaic. We conclude that demosaicking should applied first, followed by denoising. Yet we prove that this requires an adaptation of classic denoising algorithms to demosaicked noise, which we justify and specify.

1. Introduction

Most digital cameras capture image data by using a single sensor coupled with a *color filter array* (CFA). At each pixel in the array, only one color component is recorded, in a mosaic image. The most common CFA is the Bayer color array [6], in which two out of four pixels measure the green component, one measures the red and one the blue. The process of completing the missing red, green and blue values at each pixel is called demosaicking. Noise is inevitable, especially in low light conditions and for small camera sensors like those used in mobile phones. The conventional approach in raw image restoration pipelines has long been to apply denoising and demosaicking as two independent steps [49]. Furthermore, the immense majority of image processing papers addressing one of both operations do not address its combination with the other one. All classic denoising algorithms have been designed for color or grey level images with white noise added. Yet the realistic data are different: either a mosaic with white noise or a demosaicked image with structured noise.

Joint denoising/demosaicking methods. This has led several recent works to propose joint demosaicking/denoising methods [9, 21, 26, 32]. For example [22] proposed a variational model for joint demosaicking, denoising and deblurring. It uses a sparsifying prior based on wavelet packets applied to decorrelated color channels. More detail about this complex method can be found in [2].

Life has become far easier for joint denoising/demosaicking with the emergence of machine learning methods. It is, indeed, easy to simulate as much training data as needed. This methodology was used in [55] to train a *convolutional neural network (CNN)* for demosaicking outperforming the best handcrafted methods, including ARI [47], by nearly 2 decibels. One of the first joint denoising/demosaicking methods based on machine learning was proposed in [32] along with a public ground truth dataset. From there, results improved rapidly, first with deeper CNNs architectures [21], or cascaded energy minimization methods tuned by learning [37]. Then, by optimizing the perceptual quality using generative adversarial networks [15], and more recently by inserting many residual denoising layers in a CNN [38].

These joint denoising/demosaicking methods can handle a range of noise levels, but unlike traditional methods, they fail outside the trained range. The "mosaic-to-mosaic" fine-tuning introduced in [17] provides a way to adapt to unknown noise without requiring ground truth, by using bursts of raw images. The method is analogous to the noise-to-noise [42] and frame-to-frame [18] frameworks to handle noisy mosaicked raw data. However, bursts may not be available and the fine-tuning is computationally demanding.

Yet, the question of how to combine denoising and demosaicking algorithms, when conceived as independent blocks, remains very relevant. This is especially true in the context of low power or portable devices, but also given the fact that the main effort in denoising and demosaicking has

addressed them independently. In addition, they can cope with a wide range of noise levels without retraining.

A big argument in favor of performing denoising before demosaicking is that most existing demosaicking algorithms have been developed under the unrealistic assumption of noise-free data [8, 10, 21, 24, 25, 28, 33–36, 38, 43, 47, 52, 56–59, 63]. Yet the performance of these algorithms can degrade dramatically when the noise level increases on the CFA raw image. Therefore, a previous denoising step is implicitly required by these algorithms.

In this paper we focus on the early CFA processing in the imaging pipeline (operating in linear space). We assume that the noise in the raw mosaic is additive white Gaussian (AWGN) and that its variance is known. This is realistic because, first, a *variance stabilizing transform* (VST) [5] applied to a raw image results in a nearly AWG noise and, second, because an accurate noise model is often known or can be estimated [11, 53]. In general, image denoising methods can be grouped into two major categories, the model based methods such as non-local means [7, 29, 30], nlBayes [39], CBM3D [12] and WNNM [23], and deep learning methods such as [27, 60]. The ensuing CNNs are sometimes flexible in handling denoising problems with various noise levels.

Our question here is simple: Is it better to apply denoising and then demosaicking (which we will denote $DN\&DM$: DN and DM indicate denoising and demosaicking respectively), or to apply first demosaicking and then denoising ($DM\&DN$)?

DN&DM methods (*i.e.* denoising then demosaicking): advantages and drawbacks. Many state of the art works [31, 49, 50, 61] support the opinion that $DN\&DM$ outperforms $DM\&DN$. Their first convincing argument is that after demosaicking noise becomes correlated, thus losing its independent identically distributed (i.i.d.) white Gaussian property. This increases the difficulty of applying efficient denoising and actually seems to discard all classic algorithms, that mostly rely on the AGWN assumption. A second obvious argument is that the best demosaicking algorithms have been designed with noise-free images.

For example, Park *et al.* [50] considered the classic Hamilton-Adams (HA) [24] and [16] for demosaicking, combined with two denoising methods, BLS-GSM [54] and CBM3D [13]. This combination raises the question of adapting CBM3D to a CFA. To do so, the authors apply a sparsifying 4D color transform to the 4-channel image formed by rearranging the Bayer pixels. Then apply BM3D to each channel and inverse the color transform. In the very same vein, in the BM3D-CFA method [14] BM3D is applied directly on the CFA color array. To do so, "only blocks having the same CFA configuration are compared to build the 3D blocks. This is the only modification of the original BM3D". A little thought leads to the conclu-

sion that this amounts to denoise four different mosaics of the same image before aggregating the four values obtained for each pixel. The authors compare two denoising algorithms with two different setups: a) filtering CFA as a single image and b) splitting the CFA into four color components, filtering them separately, and recombining back the denoised CFA image. This paper showed a systematic improvement over [61]. They use the Zhang-Wu demosaicking method [62] for the comparisons. In our comparisons the method of [14] will be mentioned every time we consider the $DN\&DM$ setup with BM3D. We will nevertheless replace the demosaicking of [62] by RCNN [57], which clearly outperforms it.

Similarly in [9] denoising is performed by an adaptation of NL-means to the Bayer pattern, where only patches with the same CFA configuration are being matched. This paper formulates the demosaicking as a super-resolution problem, assuming that the observed values are actually averages of four values in the high resolution image. It then guides this super-resolution problem by the NL-means weights. The method is compared with [46] and [61]. The authors of [61] also propose an $DN\&DM$ method, where the demosaicking method is [62] and the the denoising method is an adaptation of nlBayes [39] to a Bayer pattern. The method extracts blocks with similar configuration in the Bayer array and groups them by similarity. Then, applies *principal component analysis* (PCA) to the groups and a Wiener denoising procedure which can be interpreted as a linear minimum mean square error estimator. In our experiments, this PCA method [61] will be considered every time we evaluate the $DN\&DM$ scheme (but combined with a more recent demosaicking such as RCNN [57]). The more recent paper [64] involves similar arguments. This paper uses a linear filter [4] to extract the luminance from the CFA. Then it remarks that this luminance is correlated, so it applies a variant of NL-means that attempts to decorrelate the noise. The same method is applied to each downsampled color channel and the high frequency of the grey level is transported back to the color channels. This method under-performs with respect to others considered here, so we shall not include it to our final comparison tables.

The paper [51] is another method promoting denoising before demosaicking, involving dictionary learning methods to remove the Poisson noise from the single channel images prior to demosaicing. Experimental results on simulated noisy images as well as real camera acquisitions, show the advantage of these methods over approaches that remove noise subsequent to demosaicing. The paper nevertheless uses [44], an outdated demosaicking method.

To summarize, in the $DN\&DM$ strategy all classic denoising algorithms such as CBM3D, nlBayes, nlMeans have been adapted to handle a noisy mosaic. Several of them [31, 49, 50, 61] address this realistic case by processing the

noisy CFA image as a half-size 4-channel color image (with one red, two green and one blue channels) and then apply a multichannel denoising algorithm to it. The advantage of the denoising step of $DN\&DM$ is that the Poisson noise can be led back by the classic case of i.i.d. white Gaussian noise by an Anscombe transform. The disadvantage is that the resolution of the image is reduced and, as a result, some details might be lost after denoising. Another issue of this strategy is that the spatial relative positions of the R, G, and B pixels are lost by handling the image as a four channel half size image.

In this paper, we address the above mentioned issues. We first delve into the advantages and disadvantages of $DN\&DM$ and $DM\&DN$ approaches. We then analyze noise properties after demosaicking and adjust two existing classic denoising algorithms (CBM3D and nlBayes) to accommodate them to this type of noise. Then, we perform a thorough experimental evaluation, to conclude that $DM\&DN$ (with an adjusted noise parameter) is superior to $DN\&DM$. This result is opposite to the conclusion of [31, 49, 50, 61]. The advantages of $DM\&DN$ seem to be linked to the fact that this scheme does not handle a half size 4-channels color image; it therefore uses the classic denoising methods directly on a full resolution color image; this results in more details being preserved and avoids checkerboard effects.

Section 2 presents in detail the problem and the main ideas behind the proposed $DM\&DN$ strategy. Section 3 is a detailed evaluation of the proposed strategy. Section 4 concludes.

2. The demosaicking and denoising framework

Consider a CFA block as shown in Fig. 1. The raw Bayer CFA images are scalar mosaics matrices with noise, which are converted to photo-finished images by the imaging pipeline. The simple pipeline proposed in [1] performs: 1. black level and dark frame correction, 2. white balance, 3. demosaicking/denoising, 4. colorspace conversion, and 5. tone curve.

Modern camera image processing chains may include multiple denoising stages, before and after the tone curve. Here, we focus on the early CFA processing of step 3. At this stage image values are linear and noise cannot be assumed white Gaussian. However, a VST leads back to the classic white Gaussian setting. When considering real images with non Gaussian noise, we shall apply a VST before the denoising step (DM) and its inverse afterwards. But, in our experiments with simulated noise we shall consider AWG noise.

Park *et al.* [50] argued that demosaicking introduces chromatic and spatial correlations to the noisy CFA image. Then the noise is no longer i.i.d. white Gaussian, which makes it harder to remove. In [31], some experiments were
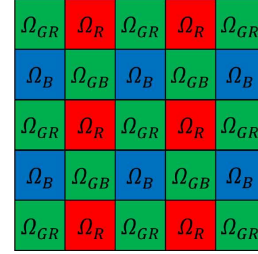

Figure 1. Bayer color filter array, CFA, which is used by most cameras.

done to show that $DN\&DM$ schemes are more efficient to suppress noise than $DM\&DN$ schemes. Based on this argument several denoising methods [3, 41, 50, 61] for raw CFA images before demosaicking were introduced. Other denoising methods that are not explicitly designed to handle raw CFA images (such as CBM3D and nlBayes) can also be applied on noisy CFA images by rearranging the CFA image into a half-size four-channels image with two greens on which the denoising algorithm is applied [50]. The denoised CFA is then recovered by undoing the pixel rearrangement. However, this strategy reduces the resolution of the image seen by the denoiser, and we observed checkerboard effects resulting from chromatic aberrations in the two green channels after denoising. To address this issue, Danielyan *et al.* [14] proposed BM3D-CFA which amounts to denoise four different mosaics of the same image before aggregating the four values obtained for each pixel.

Modeling demosaicking noise. In order to solve the above two problems, we shall revisit the $DM\&DN$ scheme which, in contrast to the $DN\&DM$ scheme, does not halve the image size. This is a way around the above mentioned problems. A serious drawback, though, is that chromatic and spatial correlations have been introduced by the demosaicking in the raw noise, which is no longer white. We must therefore analyze the *demosaicked noise*.

Definition *Given a ground truth color image* (R, G, B) *we define the* demosaicked noise *associated with a demosaicking method* DM *in the following way: first the image is mosaicked so that only one value of either* R, G, B *is kept at each pixel, according to a fixed Bayer pattern. Then white noise with standard deviation* σ_0 *is added to the mosaicked image, and the resulting noisy mosaic is demosaicked by* DM, *hence giving a noisy image* $(\tilde{R}, \tilde{G}, \tilde{B})$. *We call demosaicked noise the difference* $(\tilde{R} - R, \tilde{G} - G, \tilde{B} - B)$. *In short, it is the difference between the demosaicked version of a noisy image and its underlying ground truth.*

The model of the demosaicked noise depends on the choice of the demosaicking algorithm DM. For the demo-

(a1) Ground truth (a2) Ground truth

(b1)$DN\&DM$ /26.92dB (b2)$DN\&DM$ /26.92dB

(c1) $DM\&DN$ /25.38dB (c2) $DM\&DN$ /25.38dB

(d1) $DM\&1.5DN$ /26.95dB (d2) $DM\&1.5DN$ /26.95dB
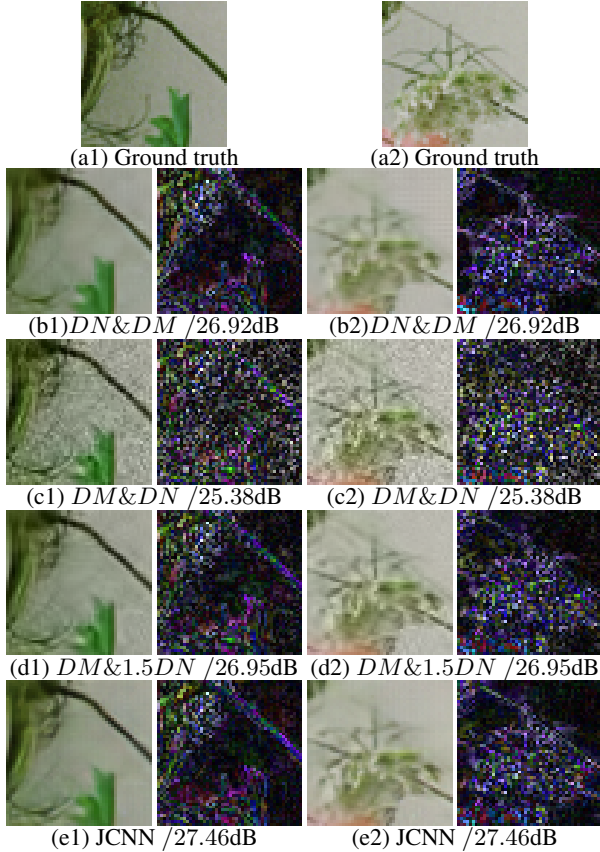
(e1) JCNN /27.46dB (e2) JCNN /27.46dB

Figure 2. Comparison of eight denoising and demosaicking schemes with noise $\sigma_0 = 20$. Left, detail of the demosaicked and denoised image; right, the difference with original that should contain mainly noise. DN: CBM3D denoising; DM: demosaicking (here we use RCNN). $1.5DN$ means that if noise level is σ_0, the input noise level parameter of denoising method DN is $\sigma = 1.5\sigma_0$; $DN\&DM$: uses the BM3D-CFA framework [14] for denoising.

saicking step we will evaluate the following state of the art methods, which have an increasing complexity: HA [24], RI [33], MLRI [34], ARI [47], LSSC [43], RCNN [57] and JCNN [21]. We are interested in algorithms with low or moderate power; only HA, RI, MLRI and RCNN have a reasonable complexity in this context. For the denoising step we shall likewise consider two classic hand-crafted algorithms, CBM3D and nlBayes.

Fig. 2 (c1) and (c2) shows an example where noisy CFA images with noise of standard deviation σ_0 were first demosaicked by RCNN and then restored by CBM3D assuming a noise parameter $\sigma = \sigma_0$. The output of CBM3D with $\sigma = \sigma_0$ has a strong residual noise. Similar results are also obtained with nlBayes (see the supplementary material). To understand empirically the right noise model to adopt after demosaicking, we simulated this $DM\&DN$ pipeline

Table 1. Denoising after demosaicking $DM\&DN$, where DN is CBM3D [13] with noise parameter equal to $C\,\sigma_0$, while noise in the raw image has standard deviation $\sigma_0 = 20$. Each row shows the CPSNR result for C ranging from 1.0 to 1.9. Each column corresponds to a different demosaicking method DM. The best result of each column is in **red**, the second best is in **green** and the third in column is in **red**, the second best is in **blue**. The best factor C for all methods is $C \simeq 1.5$, the same is true for different values of σ_0 as well (see supplementary material).

C	HA	GBTF	RI	MLRI	ARI	LSSC	RCNN
1.0	28.15	27.58	28.46	27.95	28.70	27.19	27.28
1.1	28.56	28.15	28.83	28.44	28.98	27.89	28.05
1.2	28.85	28.55	29.08	28.80	29.18	28.43	28.67
1.3	29.05	28.81	29.23	29.03	29.29	28.78	29.09
1.4	29.18	28.96	**29.31**	29.17	**29.35**	29.00	29.34
1.5	**29.23**	**29.00**	**29.32**	**29.22**	**29.35**	**29.06**	**29.41**
1.6	**29.25**	**29.01**	**29.30**	**29.23**	**29.33**	**29.06**	**29.41**
1.7	**29.25**	**28.97**	29.26	**29.20**	29.29	**29.02**	**29.36**
1.8	29.22	28.92	29.20	29.15	29.23	28.95	29.28
1.9	29.17	28.85	29.13	29.08	29.17	28.88	29.20

Table 2. RMSE between original and demosaicked image for various demosaicking algorithms in presence of noise of std σ_0.

σ_0	HA	GBTF	RI	MLRI	ARI	LSSC	RCNN
1	5.04	5.10	4.17	4.06	3.72	4.40	3.21
5	6.78	6.87	6.12	6.10	5.74	6.36	5.59
10	10.18	10.27	9.53	9.74	9.09	9.96	9.65
20	17.75	17.83	16.77	17.56	16.06	18.16	18.04
40	32.67	32.76	30.77	32.64	29.36	33.68	33.98
60	46.14	46.35	43.43	46.11	41.44	48.11	47.95

for different levels of noise σ_0, and applied CBM3D after demosaicking with a noise parameter corresponding to σ_0 multiplied by different factors $(1.0, 1.1, \cdots, 1.9)$.

The results are shown in Table 1, where the classic *color peak signal-to-noise ratio* (CPSNR) [4] is adopted as a logarithmic measure of the performance of the algorithms. It is defined by

$$\text{CPSNR}(X) = 10\log_{10}\frac{255^2}{\sum_{X=R,G,B}\text{MSE}(X)/3}, \quad \text{with}$$

$$\text{MSE}(X) = \frac{1}{|\Omega|}\sum_{(i,j)\in\Omega}(\widehat{X}(i,j) - X(i,j))^2,$$

where $\widehat{X}$ denotes the ground truth image and X is the estimated color image. From 1.0 to 1.9, the CPSNR increases first and then decreases. The best values are distributed on the lines with factors from 1.4 to 1.7. A similar behavior was also observed using nlBayes for denoising as well as for other levels of noise (see the supplementary material).
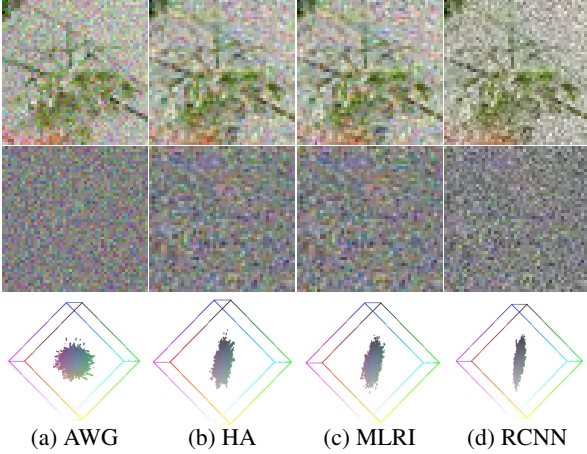
(a) AWG   (b) HA   (c) MLRI   (d) RCNN

Figure 3. AWG noise image and demosaicking noise with standard deviation $\sigma = 20$ for respectively HA, MLRI, RCNN. Last row: the color spaces (in standard (R,G,B) Cartesian coordinates) of each noise, presented in their projection with maximal area. As expected, the AWG color space is isotropic, while the color space after demosaicking is elongated in the luminance direction $Y = R + G + B$ and squeezed in the others. This amounts to an increased noise standard deviation for Y after demosaicking, and less noise in the chromatic directions.

This does not mean that the overall noise standard deviation has increased after demosaicking. Table 2 reports the standard deviation of the demosaicked noise for different noise levels. Which is estimated as the mean RMSE of demosaicked images from the McMaster-IMAX [63] dataset (Imax). We observe that for low noise ($\sigma_0 = 1$) there is a serious demosaicking error, of about 4, not caused by the noise, but by the demosaicking itself. However, for $\sigma_0 > 10$ we see that the RMSE of the demosaicked image tends to roughly 3/4 of the input noise.

At first sight, this 3/4 factor seems to contradict the observation that denoising with a parameter $1.5\sigma_0$ yields better results. This leads us to analyzing the structure of the demosaicked noise. For that we use an orthonormal Karhunen-Loève transform to maximally decorrelate the color channels [45, 48]. This type of transforms are commonly used in denoising algorithms [40] such as CBM3D and nlBayes. Here, we use a transform in which the luminance direction is $Y = \frac{R+G+B}{\sqrt{3}}$ and the orthogonal vectors C_1 and C_2 are arbitrarily chosen as in [45].

Fig. 3 shows an image contaminated with AWG noise with standard deviation $\sigma_0 = 20$ and its resulting demosaicked noise for respectively HA, MLRI, RCNN. In the last row of the figure, one can observe the color spaces (in standard (R,G,B) Cartesian coordinates) of each of these noises, each cloud being presented in its projection with maximal area. As expected, the AWG color space is isotropic and has an apparent diameter proportional to $4\sigma_0 \simeq 80$. The color

Table 3. Variance and covariance of (R, G, B) and (Y, U, V) (each first row) and the corresponding correlations (each second row) between pixels (i, j) and $(i + s, j + t)$, $s, t = 0, 1, 2$ first for AWGN (a) with standard deviation $\sigma = 20$, then for its demosaicked versions MLRI (b) and RCNN (c)

	(i,j)	(i,j+1)	(i,j+2)	(i+1,j)	(i+1,j+1)	(i+1,j+2)	(i+2,j)	(i+2,j+1)	(i+2,j+2)
R	400.6	0.6	0.4	0.7	0.1	0.7	0.3	0.2	0.8
G	401.7	0.5	1.1	0.1	0.3	0.9	1.0	0.6	0.4
B	400.2	1.2	0.1	0.5	0.6	0.0	1.9	0.3	1.9
Y	399.6	1.1	0.1	0.3	0.1	0.9	0.2	0.5	1.2
C_1	401.5	0.1	0.8	0.6	0.3	0.3	0.9	0.5	1.3
C_2	401.4	0.2	1.8	0.9	0.2	1.0	0.6	0.2	0.2

(a) AWG noise

	(i,j)	(i,j+1)	(i,j+2)	(i+1,j)	(i+1,j+1)	(i+1,j+2)	(i+2,j)	(i+2,j+1)	(i+2,j+2)
R	361.4	128.4	18.9	130.5	46.4	20.6	21.6	21.5	19.8
G	298.9	93.0	0.5	95.1	19.1	0.9	1.0	0.5	3.8
B	370.9	127.8	19.3	130.4	46.0	20.6	21.2	20.3	19.0
Y	772.2	177.7	33.0	181.3	9.6	9.2	32.6	10.9	21.4
C_1	164.8	107.1	43.7	108.8	72.8	29.3	46.1	30.2	10.1
C_2	94.3	64.4	28.1	65.8	48.2	21.9	30.3	23.1	11.1

(b) MLRI

	(i,j)	(i,j+1)	(i,j+2)	(i+1,j)	(i+1,j+1)	(i+1,j+2)	(i+2,j)	(i+2,j+1)	(i+2,j+2)
R	359.9	47.8	5.0	51.9	21.8	17.8	5.1	19.4	9.2
G	354.8	32.6	4.4	36.3	5.8	8.4	6.4	8.8	0.6
B	356.0	49.6	6.3	53.7	23.6	18.8	7.3	19.4	9.2
Y	972.3	69.0	20.8	76.4	3.6	18.6	28.9	17.3	2.2
C_1	55.1	33.8	15.3	36.0	26.1	14.6	19.0	16.6	11.8
C_2	43.3	27.3	12.3	29.4	21.5	11.7	16.0	13.7	9.4

(c) RCNN

space of the demosaicked noise is instead elongated in the luminance direction Y to about $6\sigma_0 \simeq 120$ and squeezed in the others. This amounts to an increased noise standard deviation for Y after demosaicking, and much less noise in the chromatic directions.

This is confirmed by Table 3, which shows variances and covariances of (R, G, B) and (Y, C_1, C_2) respectively for an AWG noise with $\sigma_0 = 20$, and then for the demosaicked noise obtained after demosaiciking it with MLRI and RCNN. In Table 3 (a) these statistics are computed on a pure white noise image with $\sigma = 20$. Hence the variance of Y is 400, as the $(R, G, B) \rightarrow (Y, C_1, C_2)$ transform is implemented as an isometry of $\mathbf{R}^3$. The variance of Y grows with the sophistication of the demosaicking: 772 for MLRI and 972 for RCNN. In contrast, the demosaicked noise is reduced in the chromatic axes C_1 and C_2, with a standard deviation divided by a factor between 2 and 3. But, Table 3 also shows that the residual noise on C_1 and C_2 is strongly spatially correlated, it is therefore a low frequency noise, which will require stronger filtering than white noise to be

Table 4. Covariances (each first row) and *correlations* (each second row) of the three color channels (R, G, B) of the demosaicked noise, when the initial CFA white noise satisfies $\sigma_0 = 20$.

	R	G	B		R	G	B
R	361.42	224.39	201.41	R	359.90	320.44	302.85
	1.0000	*0.6826*	*0.5501*		*1.0000*	*0.8967*	*0.8461*
G	224.39	298.94	216.86	G	320.44	354.83	299.85
	0.6826	*1.0000*	*0.6512*		*0.8967*	*1.0000*	*0.8437*
B	201.41	216.86	370.92	B	302.85	299.85	355.99
	0.5501	*0.6512*	*1.0000*		*0.8461*	*0.8437*	*1.0000*
	(a) MLRI				(b) RCNN		

Table 5. Comparison in CPSNR(dB) of average restoration performance between $DN\&DM$ and $DM\&DN$ for a fixed level of noise $\sigma_0 = 20$. We test two denoisers DN namely CBM3D, and nlBayes, and $1.5DN$ means that if noise level is σ_0, the noise level parameter for the denoising method DN is $\sigma = 1.5\sigma_0$. Both denoisers can be adapted to handle mosaics in the $DN\&DM$ schemes (see in the text). The best result of each column is marked with a box. The best result of each line is in **red** and the second best one is in green.

DN	Algorithm	HA	RI	MLRI	ARI	RCNN
CBM3D	$DN\&DM$	28.11	28.45	27.97	**28.69**	27.27
	$DM\&DN$	28.15	28.46	27.95	**28.70**	27.28
	$DM\&1.5DN$	29.24	29.32	29.22	29.36	**29.41**
nlBayes	$DN\&DM$	28.17	28.17	28.17	28.18	**28.28**
	$DM\&DN$	28.67	28.99	28.57	**29.21**	28.02
	$DM\&1.5DN$	29.29	29.26	29.22	29.31	**29.36**

removed. This table also shows that the Y component of the demosaicked noise remains almost white.

This leads to a simple conclusion: since image denoising algorithms are guided by the Y component [13, 39], we can denoise with methods designed for white noise, but with a noise parameter adapted to the increased variance of Y.

To understand why the variance of Y is far larger than the AWG noise it comes from, let us study in Table 4 the correlation between the three channels (R, G, B) in the demosaicked noise of MLRI and RCNN. We observe a strong (R, G, B) correlation, which is caused by the "tendency to grey" of all demosaicking algorithms. Assuming that the demosaicked noisy pixel components (denoted $\widetilde{\epsilon}_R, \widetilde{\epsilon}_G, \widetilde{\epsilon}_B$) have a correlation coefficient close to 1 then we have

$$Y = \frac{\widetilde{\epsilon}_R + \widetilde{\epsilon}_G + \widetilde{\epsilon}_B}{\sqrt{3}} \sim \sqrt{3}\, N(0, \sigma_0).$$

This factor of about 1.7 corresponds to the case with maximum correlation. Our observation of an optimal factor near 1.5 responds to a lower correlation between the colors.

3. Experimental evaluation

We evaluated the proposed framework using two classic noise free color image datasets: Kodak [20] and Imax [63], composed on 18 and 25 images respectively. We also evaluated it on a set of 14 real raw images from the SIDD dataset [1], which comes with ground truth acquisitions.

Evaluation of DN&DM and DM&DN strategies. We performed simulations with the schemes: $DN\&DM$ and $DM\&DN$. The considered demosaicking methods range from classic to very modern: HA[24], RI[33], MLRI[34], ARI [47], and RCNN[57]. For the denoising stage two classic hand-crafted patch-based denoising algorithms were considered: CBM3D [13] and nlBayes [39]. As commented in the introduction, both methods can be adapted to handle mosaics (in the $DN\&DM$ setting). In the case of CBM3D this amounts to applying the method by Danielyan *et al.* [14], while for nlBayes this is done by denoising the 4-channel image associated to the mosaic. The schemes were applied the mosaic images of the Imax dataset corrupted by AWGN with standard deviations $\sigma_0 \in [1, \cdots, 60]$.

From Table 5, we can see that $DM\&DN$ with parameter $\sigma = \sigma_0$ is not better than $DN\&DM$, but $DM\&1.5DN$ (which denotes denoising DN with parameter $\sigma = 1.5\sigma_0$) beats clearly $DN\&DM$. Other values of σ_0 are shown in the supplementary material, though with similar behavior. This might explain why many researchers think that the scheme $DN\&DM$ was superior to the scheme $DM\&DN$.

In addition to the good CPSNR results, one important advantage of the $DM\&DN$ schemes is the high visual quality of the final restored images. Fig. 2 demonstrates the differences between the various solutions (based on BM3D) obtained on image #3 of the Imax dataset. To save space, only crops of the full-color results and corresponding differences with the ground truth are shown here.

The $DN\&DM$ scheme shown in Fig. 2 (b1) and (b2) uses BM3D-CFA [14] for denoising; we can observe some minor checkerboard artifacts. From Fig. 2 (c1) and (c2), we can deduce that there is no checkerboard effect but that much noise remains in the restored image by $DM\&DN$ schemes with parameter $1.0\sigma_0$. The result of $DM\&1.5DN$ (Fig. 2 (d1) and (d2)) are smooth without checkerboard effects. Fig. 2 (e1) and (e2) correspond to the outputs of the CNN joint denoising and demosaicking method JCNN [21].

One can observe thin structures in the upper left corner of Fig. 2 (a1), but they disappear in the restored image by $DN\&DM$. The proposed $DM\&1.5DN$ scheme restores them. The second column of Fig. 2 illustrates a similar situation in which thin details are recovered by $DM\&DN$ and $DM\&1.5DN$ but not in the others.

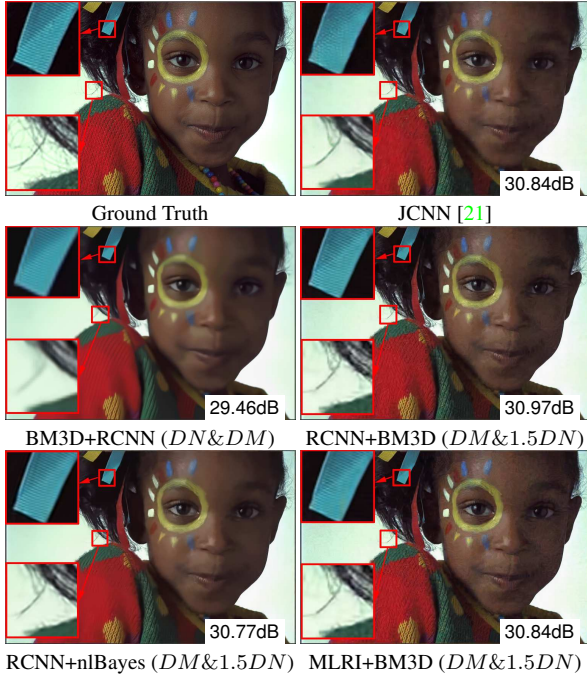In short, it appears that the $DM\&DN$ scheme with an appropriate parameter (namely $DM\&1.5DN$) outperforms

Figure 4. Demosaicking and denoising results on an image from the Kodak dataset with $\sigma = 20$. We compare a $DN\&DM$ scheme BM3D+RCNN [14], with three $DM\&1.5DN$: RCNN+CBM3D, RCNN+nlBayes and MLRI+BM3D. As a reference we also include the result of a joint CNN method JCNN [21]. (Limited to $\sigma \leq 20$, as the network is not trained beyond that level.)

the competition in terms of visual quality. This is due to the fact that it efficiently uses spatial and spectral image characteristics to remove noise, preserve edges and fine details. Indeed, contrary to the $DN\&DM$ schemes, $DM\&1.5DN$ does not reduce the resolution of the noisy image. Using an $DN\&DM$ scheme ends up over-smoothing the result. It comes to no surprise that JCNN performs slightly better than the other methods; however, it is much more computationally demanding and only works for $\sigma \leq 20$.

In a systematic comparison between the schemes involving CBM3D and nlBayes, schemes with CBM3D proved to perform slightly better. Furthermore, CBM3D is about four times faster than nlBayes. Hence, the following experiments are more focused on CBM3D.

Comparison with methods from the literature. To complete this comparison we went back to all $DN\&DM$ schemes proposed in the literature, and performed a systematic comparison for the two classic Kodak and Imax datasets. These databases are always used in demosaicking evaluations, because they illustrate different challenges of the demosaicking problem, Imax being difficult by its color contrast, and Kodak challenging for the recovery of fine structure. In Tables 6 and 7 we compare rep-

resentative $DN\&DM$ methods from the literature with the best $DM\&DN$ methods identified above (all of them $DM\&1.5DN$):

– The two best $DM\&1.5DN$ from on Table 5 are considered. Namely, RCNN for demosaicking followed by CBM3D (denoted *RCNN+CBM3D*) or nlBayes (*RCNN+nlBayes*) for denoising.

– We also consider a "low-cost" $DM\&1.5DN$ combination using MLRI [34] for demosaicking and CBM3D for denoising (*MLRI+CBM3D*).

The considered $DN\&DM$ methods from the literature are:

– The BM3D-CFA algorithm proposed in [14] to avoid the checkerboard effects resulting from independently applying BM3D to the color phases of CFA images. We evaluate BM3D-CFA [14] followed by Hamilton Adams demosaicking (*BM3D+HA*), as well as followed by a state-of-the-art RCNN demosaicking [57] (*BM3D+RCNN*).

– The Park *et al.* [50] CFA denoising framework applying PCA to the RGB color space in the Kodak dataset and then removing noise in each channel by BM3D. This preprocessing is advantageous for the Kodak image set, but inadequate for the Imax image set. We evaluate this framework [50] with BM3D [12] followed by the RCNN demosaicking [57] (*Park+RCNN*).

– The PCA-CFA method proposed in [61] is a spatially-adaptive denoising based on principal component analysis (PCA) that exploits the spatial and spectral correlations of CFA images to preserve color edges and details. We evaluate PCA-CFA [61] followed by DLMM demosaiciking [62] (*PCA+DLMM*) and RCNN demosaicking [57] (*PCA+RCNN*).

– Finally, as a reference, we include the CNN-based joint denoising and demosaicking (*JCNN*) of [19, 21]. But its results are only available for noise with $\sigma \leq 20$ because the network is not trained beyond that level.

From Tables 6 and 7 we see that the $DM\&DN$ method RCNN+CBM3D as well as RCNN+nlBayes yield the best results on the Kodak dataset, and the margin with respect to the best $DN\&DM$ method (BM3D+RCNN, i.e. BM3D-CFA [13] with RCNN [57]) is quite large: more than 1.5dB on average. In Fig. 3 we compare some results obtained on an image from the Kodak dataset. From the upper-left extract we can see that textures are better restored with RCNN+CBM3D and MLRI+CBM3D, while JCNN introduces some defects. From the extract we see that the $DM\&1.5DN$ methods preserve much more details than BM3D+RCNN, and the result is comparable to JCNN.

On the Imax database RCNN+CBM3D has the highest CPSNRs on high noise levels, by a small gap though.

Table 6. Comparison of the results (CPSNR in dB) between different denoising and demosaicking methods for the **Imax** image set. The best result of each line is in **red**, the second best one is in **green** and the third best one is in **blue**.

σ	DN&DM					DM&1.5DN			JCNN
	BM3D + HA	BM3D + RCNN	Park + RCNN	PCA + DLMM	PCA + RCNN	RCNN + CBM3D	RCNN + nlBayes	MLRI + CBM3D	
1	34.63	38.53	35.37	33.99	37.52	38.36	38.42	36.52	38.59
5	33.43	35.62	32.86	32.69	34.87	35.39	35.29	34.60	33.48
10	31.84	32.92	30.06	30.73	31.89	32.75	32.59	32.36	33.09
20	29.22	29.55	26.86	27.57	27.99	29.41	29.25	29.22	29.79
40	25.50	25.51	23.86	23.50	23.57	25.52	25.09	25.39	–
60	21.55	21.34	21.75	20.89	20.89	22.78	22.31	22.63	–
Av	28.09	28.88	26.89	26.71	27.53	28.99	28.72	28.58	–

Table 7. Comparison of the results (CPSNR in dB) between different denoising and demosaicking methods for the **Kodak** image set. The best result of each line is in **red**, the second best one is in **green** and the third best one is in **blue**.

σ	DN&DM					DM&1.5DN			JCNN
	BM3D + HA	BM3D + RCNN	Park + RCNN	PCA + DLMM	PCA + RCNN	RCNN + CBM3D	RCNN + nlBayes	MLRI + CBM3D	
1	34.70	40.55	40.36	38.19	39.12	40.98	40.98	38.52	41.15
5	32.84	34.89	34.87	34.99	35.42	36.55	36.42	35.71	34.13
10	30.34	30.93	30.85	31.83	32.01	33.36	33.18	32.94	33.27
20	27.59	27.70	27.42	28.11	28.14	29.98	29.87	29.70	29.95
40	24.79	24.78	24.88	24.15	24.08	26.71	26.29	26.44	–
60	22.58	22.55	23.19	21.77	21.70	24.42	23.93	24.16	–
Av	27.47	28.35	28.36	27.96	28.09	30.19	29.93	29.64	–

For low noise levels BM3D+RCNN is better, but the difference with RCNN+CBM3D is very small. The joint denoising-demosaicking network JCNN [21] yield the best results on the Imax dataset for $\sigma \leq 20$ yet, the margin with respect to RCNN+CBM3D is again small. Overall, by looking at the average CPSNR we can say that RCNN+CBM3D ($DM\&1.5DN$) is indeed much more robust than BM3D+RCNN.

Evaluation on real images. We evaluated on a set of 14 raw images taken from the Small SIDD dataset [1]. For simplicity, the selected images correspond to phones from the same manufacturer. We adopted the simple pipeline proposed by the authors, which yields photo finished images that can be compared with the ground truth. The considered methods (RCNN+CBM3D, CBM3D+RCNN, and JCNN) were applied at the demosaicking stage (in linear space). Before any denoising step (DN) we applied a VST (squared root [5]), which whitens the noise, and invert it afterwards.
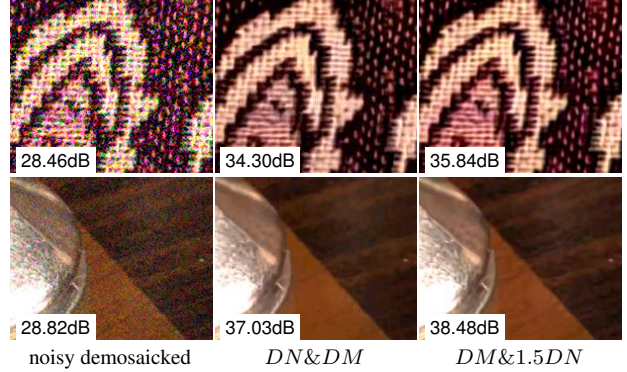

Figure 5. Details of a real images (enhanced contrast) from the SIDD [1] dataset. From left to right: noisy input (demosaicked), BM3D+RCNN , and RCNN+CBM3D.

Table 8. Average CPSNR over 14 raw images taken from the Small SIDD dataset [1]. The reported average noise level is scaled to the range 0-255.

mean σ	CBM3D+RCNN	RCNN+CBM3D	JCNN
7.65	38.19	**39.64**	38.54

The noise level was estimated using [11] and provided to the denoising algorithms and JCNN.

Table 8 reports the average CPSNR obtained on these images and the average of the estimated noise levels (after whitening). These values are consistent with the simulated results obtained on the Kodak database (Table 7). The result in Fig. 5, and the supplementary material, support the case in favor of the $DM\&1.5DN$ schemes (RCNN+CBM3D).

4. Conclusions

This paper analyzed the advantages and disadvantages of denoising before demosaicking ($DN\&DM$) schemes, versus demosaicking before denoising ($DM\&DN$), to recover high quality full-color images. We showed that for the $DM\&DN$ schemes a very simple change of the noise parameter of the denoiser DN coped with the structure of demosaicked noise, and led to efficient denoising *after* demosaicking. This has allowed a better preservation of fine structures often smoothed by the $DN\&DM$ schemes. Our best performing combination in terms of quality and speed is a $DM\&1.5DN$ scheme, where demosaicking DM is done by a fast algorithm RCNN [57] followed by CBM3D denoising $1.5DN$ with noise parameter equal to $1.5\sigma_0$. Nevertheless, we anticipate joint demosaicking and denoising methods obtained by deep learning to win the end game when they become more compact or rapid.

References

[1] Abdelrahman Abdelhamed, Stephen Lin, and Michael S. Brown. A High-Quality Denoising Dataset for Smartphone Cameras. In *2018 IEEE/CVF Conference on Computer Vision and Pattern Recognition*, pages 1692–1700. IEEE, jun 2018. 3, 6, 8

[2] Jan Aelterman, Bart Goossens, Jonas De Vylder, Aleksandra Pižurica, and Wilfried Philips. Computationally efficient locally adaptive demosaicing of color filter array images using the dual-tree complex wavelet packet transform. *PloS one*, 8(5):e61846, 2013. 1

[3] Hiroki Akiyama, Masayuki Tanaka, and Masatoshi Okutomi. Pseudo four-channel image denoising for noisy cfa raw data. In *2015 IEEE International Conference on Image Processing (ICIP)*, pages 4778–4782. IEEE, 2015. 3

[4] David Alleysson, Sabine Susstrunk, and Jeanny Hérault. Linear demosaicing inspired by the human visual system. *IEEE Transactions on Image Processing*, 14(4):439–449, 2005. 2, 4

[5] F. J. Anscombe. The Transformation of Poisson, Binomial and Negative-Binomial Data. *Biometrika*, 35(3/4):246, dec 1948. 2, 8

[6] Bryce E Bayer. Color imaging array, July 20 1976. US Patent 3,971,065. 1

[7] Antoni Buades, Bartomeu Coll, and Jean-Michel Morel. A review of image denoising algorithms, with a new one. *Multiscale Modeling & Simulation*, 4(2):490–530, 2005. 2

[8] Antoni Buades, Bartomeu Coll, Jean-Michel Morel, and Catalina Sbert. Self-similarity driven demosaicking. *Image Processing On Line*, 1:51–56, 2011. 2

[9] Priyam Chatterjee, Neel Joshi, Sing Bing Kang, and Yasuyuki Matsushita. Noise suppression in low-light images through joint denoising and demosaicing. In *CVPR 2011*, pages 321–328. IEEE, 2011. 1, 2

[10] Xiangdong Chen, Liwen He, Gwanggil Jeon, and Jechang Jeong. Multidirectional weighted interpolation and refinement method for bayer pattern cfa demosaicking. *IEEE Transactions on Circuits and Systems for Video Technology*, 25(8):1271–1282, 2015. 2

[11] Miguel Colom and Antoni Buades. Analysis and Extension of the Ponomarenko et al. Method, Estimating a Noise Curve from a Single Image. *Image Processing On Line*, 3:173–197, 2013. 2, 8

[12] Kostadin Dabov, Alessandro Foi, Vladimir Katkovnik, and Karen Egiazarian. Image denoising with block-matching and 3d filtering. In *Image Processing: Algorithms and Systems, Neural Networks, and Machine Learning*, volume 6064, page 606414. International Society for Optics and Photonics, 2006. 2, 7

[13] Kostadin Dabov, Alessandro Foi, Vladimir Katkovnik, and Karen Egiazarian. Color image denoising via sparse 3d collaborative filtering with grouping constraint in luminance-chrominance space. In *2007 IEEE International Conference on Image Processing*, volume 1, pages I–313. IEEE, 2007. 2, 4, 6, 7

[14] Aram Danielyan, Markku Vehvilainen, Alessandro Foi, Vladimir Katkovnik, and Karen Egiazarian. Cross-color bm3d filtering of noisy raw data. In *2009 international workshop on local and non-local approximation in image processing*, pages 125–129. IEEE, 2009. 2, 3, 4, 6, 7

[15] Weishong Dong, Ming Yuan, Xin Li, and Guangming Shi. Joint demosaicing and denoising with perceptual optimization on a generative adversarial network. *arXiv preprint arXiv:1802.04723*, 2018. 1

[16] Eric Dubois. Frequency-domain methods for demosaicking of bayer-sampled color images. *IEEE Signal Processing Letters*, 12(12):847–850, 2005. 2

[17] Thibaud Ehret, Axel Davy, Pablo Arias, and Gabriele Facciolo. Joint demosaicing and denoising by overfitting of bursts of raw images. In *ICCV 2019*, 2019. 1

[18] Thibaud Ehret, Axel Davy, Jean-Michel Morel, Gabriele Facciolo, and Pablo Arias. Model-blind Video Denoising Via Frame-to-frame Training. In *CVPR 2019*, pages 11369–11378, 2019. 1

[19] Thibaud Ehret and Gabriele Facciolo. A Study of Two CNN Demosaicking Algorithms. *Image Processing On Line*, 9:220–230, 2019. 7

[20] Rick Franzen. Kodak lossless true color image suite, 2012. 6

[21] Michaël Gharbi, Gaurav Chaurasia, Sylvain Paris, and Frédo Durand. Deep joint demosaicking and denoising. *ACM Transactions on Graphics (TOG)*, 35(6):191, 2016. 1, 2, 4, 6, 7, 8

[22] Bart Goossens, Hiep Luong, Jan Aelterman, Aleksandra Pizurica, and Wilfried Philips. An overview of state-of-the-art denoising and demosaicking techniques: toward a unified framework for handling artifacts during image reconstruction. In *Image Sensor Workshop*, 2015. 1

[23] Shuhang Gu, Lei Zhang, Wangmeng Zuo, and Xiangchu Feng. Weighted nuclear norm minimization with application to image denoising. In *Proceedings of the IEEE conference on computer vision and pattern recognition*, pages 2862–2869, 2014. 2

[24] John F Hamilton Jr and James E Adams Jr. Adaptive color plan interpolation in single sensor color electronic camera, May 13 1997. US Patent 5,629,734. 2, 4, 6

[25] Kaiming He, Jian Sun, and Xiaoou Tang. Guided image filtering. *IEEE transactions on pattern analysis & machine intelligence*, (6):1397–1409, 2013. 2

[26] Keigo Hirakawa and Thomas W Parks. Joint demosaicing and denoising. *IEEE Transactions on Image Processing*, 15(8):2146–2157, 2006. 1

[27] Viren Jain and Sebastian Seung. Natural image denoising with convolutional networks. In *Advances in neural information processing systems*, pages 769–776, 2009. 2

[28] Sunil Prasad Jaiswal, Oscar C Au, Vinit Jakhetiya, Yuan Yuan, and Haiyan Yang. Exploitation of inter-color correlation for color image demosaicking. In *2014 IEEE International Conference on Image Processing (ICIP)*, pages 1812–1816. IEEE, 2014. 2

[29] Qiyu Jin, Ion Grama, Charles Kervrann, and Quansheng Liu. Nonlocal means and optimal weights for noise removal. *SIAM Journal on Imaging Sciences*, 10(4):1878–1920, 2017. 2

[30] Qiyu Jin, Ion Grama, and Quansheng Liu. Convergence theorems for the non-local means filter. *Inverse Problems & Imaging*, 12(4):853–881, 2018. 2

[31] Ossi Kalevo and Henry Rantanen. Noise reduction techniques for bayer-matrix images. In *Sensors and Camera Systems for Scientific, Industrial, and Digital Photography Applications III*, volume 4669, pages 348–359. International Society for Optics and Photonics, 2002. 2, 3

[32] Daniel Khashabi, Sebastian Nowozin, Jeremy Jancsary, and Andrew W Fitzgibbon. Joint demosaicing and denoising via learned nonparametric random fields. *IEEE Transactions on Image Processing*, 23(12):4968–4981, 2014. 1

[33] Daisuke Kiku, Yusuke Monno, Masayuki Tanaka, and Masatoshi Okutomi. Residual interpolation for color image demosaicking. In *2013 IEEE International Conference on Image Processing*, pages 2304–2308. IEEE, 2013. 2, 4, 6

[34] Daisuke Kiku, Yusuke Monno, Masayuki Tanaka, and Masatoshi Okutomi. Minimized-laplacian residual interpolation for color image demosaicking. In *Digital Photography X*, volume 9023, page 90230L. International Society for Optics and Photonics, 2014. 4, 6, 7

[35] Daisuke Kiku, Yusuke Monno, Masayuki Tanaka, and Masatoshi Okutomi. Beyond color difference: Residual interpolation for color image demosaicking. *IEEE Transactions on Image Processing*, 25(3):1288–1300, 2016.

[36] Yonghoon Kim and Jechang Jeong. Four-direction residual interpolation for demosaicking. *IEEE Transactions on Circuits and Systems for Video Technology*, 26(5):881–890, 2016. 2

[37] Teresa Klatzer, Kerstin Hammernik, Patrick Knobelreiter, and Thomas Pock. Learning joint demosaicing and denoising based on sequential energy minimization. In *2016 IEEE International Conference on Computational Photography (ICCP)*, pages 1–11. IEEE, 2016. 1

[38] Filippos Kokkinos and Stamatios Lefkimmiatis. Iterative joint image demosaicking and denoising using a residual denoising network. *IEEE Transactions on Image Processing*, 2019. 1, 2

[39] Marc Lebrun, Antoni Buades, and Jean-Michel Morel. A nonlocal bayesian image denoising algorithm. *SIAM Journal on Imaging Sciences*, 6(3):1665–1688, 2013. 2, 6

[40] M Lebrun, M Colom, A Buades, and J M Morel. Secrets of image denoising cuisine. *Acta Numerica*, 21:475–576, may 2012. 5

[41] Min Lee, Sang Park, and Moon Kang. Denoising algorithm for cfa image sensors considering inter-channel correlation. *Sensors*, 17(6):1236, 2017. 3

[42] Jaakko Lehtinen, Jacob Munkberg, Jon Hasselgren, Samuli Laine, Tero Karras, Miika Aittala, and Timo Aila. Noise2Noise: Learning Image Restoration without Clean Data. In *35th International Conference on Machine Learning, ICML 2018*, 2018. 1

[43] Julien Mairal, Francis R Bach, Jean Ponce, Guillermo Sapiro, and Andrew Zisserman. Non-local sparse models for image restoration. In *ICCV*, volume 29, pages 54–62. Citeseer, 2009. 2, 4

[44] Henrique S Malvar, Li-wei He, and Ross Cutler. High-quality linear interpolation for demosaicing of bayer-patterned color images. In *2004 IEEE International Conference on Acoustics, Speech, and Signal Processing*, volume 3, pages iii–485. IEEE, 2004. 2

[45] Henrique S. Malvar, Gary J. Sullivan, and Sridhar Srinivasan. Lifting-based reversible color transformations for image compression. In Andrew G. Tescher, editor, *Applications of Digital Image Processing XXXI*, page 707307, aug 2008. 5

[46] Daniele Menon and Giancarlo Calvagno. Joint demosaicking and denoisingwith space-varying filters. In *2009 16th IEEE International Conference on Image Processing (ICIP)*, pages 477–480. IEEE, 2009. 2

[47] Yusuke Monno, Daisuke Kiku, Masayuki Tanaka, and Masatoshi Okutomi. Adaptive residual interpolation for color and multispectral image demosaicking. *Sensors*, 17(12):2787, 2017. 1, 2, 4, 6

[48] Yu-Ichi Ohta, Takeo Kanade, and Toshiyuki Sakai. Color information for region segmentation. *Computer Graphics and Image Processing*, 13(3):222–241, jul 1980. 5

[49] Dmitriy Paliy, Mejdi Trimeche, Vladimir Katkovnik, and Sakari Alenius. Demosaicing of noisy data: spatially adaptive approach. In *Image Processing: Algorithms and Systems V*, volume 6497, page 64970K. International Society for Optics and Photonics, 2007. 1, 2, 3

[50] Sung Hee Park, Hyung Suk Kim, Steven Lansel, Manu Parmar, and Brian A Wandell. A case for denoising before demosaicking color filter array data. In *2009 Conference Record of the Forty-Third Asilomar Conference on Signals, Systems and Computers*, pages 860–864. IEEE, 2009. 2, 3, 7

[51] Sukanya Patil and Ajit Rajwade. Poisson noise removal for image demosaicing. In *BMVC*, 2016. 2

[52] Ibrahim Pekkucuksen and Yucel Altunbasak. Gradient based threshold free color filter array interpolation. In *Image Processing (ICIP), 2010 17th IEEE International Conference on*, pages 137–140. IEEE, 2010. 2

[53] Nikolay Ponomarenko, Vladimir V. Lukin, Mikhail Zriakhov, Arto Kaarna, and Jaakko T. Astola. An automatic approach to lossy compression of AVIRIS images. In *Geoscience and Remote Sensing Symposium, 2007. IGARSS 2007. IEEE International*, pages 472–475. IEEE, 2007. 2

[54] Javier Portilla, Vasily Strela, Martin J Wainwright, and Eero P Simoncelli. Image denoising using scale mixtures of gaussians in the wavelet domain. *IEEE Trans Image Processing*, 12(11), 2003. 2

[55] Nai-Sheng Syu, Yu-Sheng Chen, and Yung-Yu Chuang. Learning deep convolutional networks for demosaicing. *arXiv preprint arXiv:1802.03769*, 2018. 1

[56] Daniel Stanley Tan, Wei-Yang Chen, and Kai-Lung Hua. Deepdemosaicking: Adaptive image demosaicking via multiple deep fully convolutional networks. *IEEE Transactions on Image Processing*, 27(5):2408–2419, 2018. 2

[57] Runjie Tan, Kai Zhang, Wangmeng Zuo, and Lei Zhang. Color image demosaicking via deep residual learning. In *IEEE Int. Conf. Multimedia and Expo (ICME)*, 2017. 2, 4, 6, 7, 8

[58] Lei Wang and Gwanggil Jeon. Bayer pattern cfa demosaicking based on multi-directional weighted interpolation and guided filter. *IEEE Signal Processing Letters*, 22(11):2083–2087, 2015.

[59] Jiqing Wu, Radu Timofte, and Luc Van Gool. Demosaicing based on directional difference regression and efficient regression priors. *IEEE transactions on image processing*, 25(8):3862–3874, 2016. 2

[60] Kai Zhang, Wangmeng Zuo, Yunjin Chen, Deyu Meng, and Lei Zhang. Beyond a gaussian denoiser: Residual learning of deep cnn for image denoising. *IEEE Transactions on Image Processing*, 26(7):3142–3155, 2017. 2

[61] Lei Zhang, Rastislav Lukac, Xiaolin Wu, and David Zhang. Pca-based spatially adaptive denoising of cfa images for single-sensor digital cameras. *IEEE transactions on image processing*, 18(4):797–812, 2009. 2, 3, 7

[62] Lei Zhang and Xiaolin Wu. Color demosaicking via directional linear minimum mean square-error estimation. *IEEE Transactions on Image Processing*, 14(12):2167–2178, 2005. 2, 7

[63] Lei Zhang, Xiaolin Wu, Antoni Buades, and Xin Li. Color demosaicking by local directional interpolation and nonlocal adaptive thresholding. *Journal of Electronic imaging*, 20(2):023016, 2011. 2, 5, 6

[64] Xingyu Zhang, Ming-Ting Sun, Lu Fang, and Oscar C Au. Joint denoising and demosaicking of noisy cfa images based on inter-color correlation. In *2014 IEEE International Conference on Acoustics, Speech and Signal Processing (ICASSP)*, pages 5784–5788. IEEE, 2014. 2